Conformational Stability of Factor VIIa: Biophysical Studies of Thermal and Guanidine Hydrochloride-Induced Denaturation

Per-Ola Freskgård,*,‡ Lars C. Petersen,‡ Don A. Gabriel,§ Xiao Li,§ and Egon Persson*,‡

Vessel Wall Biology, Health Care Discovery, Novo Nordisk A/S, Niels Steensens Vej 1, DK-2820 Gentofte, Denmark, and Center for Thrombosis and Hemostasis and Division of Hematology/Oncology, University of North Carolina School of Medicine, Chapel Hill, North Carolina 27599

Received November 19, 1997; Revised Manuscript Received March 9, 1998

ABSTRACT: The binding of the multidomain protein factor VIIa (fVIIa) to tissue factor provides the interprotein communication necessary to make fVIIa an efficient catalyst of the initial event in the extrinsic pathway of blood coagulation. We have investigated the stability of individual domains in fVIIa and the influence of Ca^{2+} and an irreversible active-site inhibitor (FFR-chloromethyl ketone). Equilibrium guanidine hydrochloride (GuHCl)-induced unfolding monitored by tryptophan fluorescence and far-UV circular dichroism (CD) demonstrated that the γ-carboxyglutamic acid (Gla) domain unfolds at 0.3 M GuHCl and the serine protease (SP) domain at 3 M GuHCl and that Ca^{2+} is a prerequisite for the formation of an ordered, compact structure in the Gla domain. The loss of amidolytic activity coincides with the first transition, which is stabilized by the active-site inhibitor, and a change in the environment of the active site is demonstrated using a fluorescent inhibitor (DEGR-chloromethyl ketone). Thermal unfolding monitored by differential scanning calorimetry (DSC) reveals that Ca^{2+} stabilizes the SP domain slightly, increasing the unfolding temperature by 2.7 °C. In addition, Ca^{2+} is required for a large enthalpy change concomitant with unfolding of the Gla domain, and this unfolding enthalpy is only detectable in the presence of the SP domain, indicating some kind of interaction between these domains. Thermal unfolding measured by CD indicates secondary structural changes at the same temperature as the heat absorption in the DSC but only when both the Gla domain and the SP domain are present together with Ca^{2+} ions. Taken together, these results indicate a Ca^{2+}-dependent interaction between the Gla domain and the SP domain, implying a high degree of flexibility of the domains in free fVIIa. It is also shown that the epidermal growth factor-like domains are stable at elevated temperatures and high GuHCl concentrations. Moreover, already at physiological temperature, subtle structural changes take place which influence the overall shape of fVIIa and are detrimental to its enzymatic activity.

Coagulation factor VIIa (fVIIa)[1] is a vitamin K-dependent glycoprotein which, in complex with its receptor and cofactor tissue factor (TF), initiates the blood coagulation cascade (*1*). The majority of the proteins involved in coagulation and anticoagulation are so-called mosaic proteins composed of multiple domains (*2*). This architecture allows separate functions, such as protein binding and activity, to be optimally exerted by different domains which are assembled into a single, highly specialized protein. fVIIa contains 406 amino acid residues divided between a light chain (residues 1−152) and a heavy chain (residues 153−406). The light chain contains a domain rich in γ-carboxyglutamic acid (Gla) residues (Gla domain), followed by two epidermal growth factor (EGF)-like domains. The heavy chain includes the catalytic triad and shares the fold of the chymotrypsin-like serine proteases. It is referred to as the serine protease (SP) domain, and its primary responsibility is to convert the coagulation factors IX and X from zymogens to active enzymes (*3*, *4*). The interaction between fVIIa and TF has been studied extensively using a variety of techniques. It has been established that fVIIa interacts directly with TF with three of its four domains (*5*, *6*). The Gla and EGF-like domains are required for protein−protein and protein−membrane interactions responsible for complex formation between fVIIa and TF on the cell membrane. The light chain, primarily the first EGF-like domain, contributes the majority of the binding energy (*7*). The strong binding of this region to TF positions the SP domain for the interaction with TF responsible for enhancement of the fVIIa protease activity. It has also been shown that fVIIa coordinates Ca^{2+} ions in three distinct regions with different affinities and that Ca^{2+} binding is a prerequisite for high-affinity binding of fVIIa to TF (*8*, *9*).

* Authors to whom correspondence should be addressed. P.-O. F.: phone, +45 4443 9742; fax, +45 4443 8092; e-mail, pof@novo.dk. E.P.: phone, +45 4443 9731; fax, +45 4443 8092; e-mail, egpe@novo.dk.

‡ Novo Nordisk A/S.

§ University of North Carolina School of Medicine.

[1] Abbreviations: CD, circular dichroism; DSC, differential scanning calorimetry; QLS, quasi-elastic light scattering; fVIIa, factor VIIa; des-(1−44)-fVIIa, fVIIa lacking the 44 N-terminal amino acids; fVII-GlaEGF$_{NC}$, fVIIa fragment containing amino acid residues 1−144 and 248−266; SP, serine protease; FFR-fVIIa, fVIIa inhibited with Phe-Phe-Arg chloromethyl ketone; DEGR-fVIIa, fVIIa inhibited with dansyl-Glu-Gly-Arg chloromethyl ketone; TF, tissue factor; GuHCl, guanidine hydrochloride; Gla, γ-carboxyglutamic acid; EGF, epidermal growth factor.

S0006-2960(97)02847-X CCC: $15.00
Published on Web 04/29/1998

The structure of fVIIa in the absence of TF remains unknown, since it cannot be directly inferred from the structure seen in the complex. An X-ray and neutron scattering study suggests an extended structure of fVIIa in solution (*10*), with the domains ordered like pearls on a string, whereas recent studies on other homologous coagulation proteins, factor IX and protein C, suggest interdomain interactions (*11*, *12*). A more detailed study is needed to elucidate the structural organization and stability of the domains in fVIIa.

We have characterized fVIIa using various biophysical techniques, including differential scanning calorimetry (DSC), circular dichroism (CD), fluorescence spectroscopy, and quasi-elastic light scattering (QLS). Different fragments of fVIIa have been used in this study to allow us to assign changes in the structure upon denaturation to individual domains and thus to obtain information about their intrinsic stability. In particular, the role of Ca^{2+} in the overall stability of fVIIa has been investigated, but also investigated was the effect of an irreversible active-site inhibitor. We found that fVIIa unfolds in at least two distinct transitions when using guanidine hydrochloride (GuHCl) as the denaturant, the Gla domain being less stable than the SP domain. Analyses of the thermal stability of fVIIa by DSC and CD reveal only one major unfolding transition that is dependent on a Ca^{2+}-loaded Gla domain and the presence of the SP domain, which is an indication of a domain−domain interaction. Moreover, subtle structural changes occur in fVIIa prior to the major unfolding transition.

EXPERIMENTAL PROCEDURES

Proteins. Human recombinant fVIIa was produced as described (*13*), and Phe-Phe-Arg (FFR)-fVIIa (*14*) and dansyl-Glu-Gly-Arg (DEGR)-fVIIa were obtained by incubation with the respective chloromethyl ketone. The des-(1−44)-fVIIa fragment containing residues 45−406 (*15*) and the fVII-GlaEGF$_{NC}$ fragment containing residues 1−144 and 248−266 (*16*) were prepared as described. The molar extinction coefficients (molecular weights in parantheses) for the fVIIa variants given below were calculated using the algorithm of Pace et al. (*17*): fVIIa, FFR-fVIIa, and DEGR-fVIIa, 63 380 (50 000); des(1−44)-fVIIa, 56 265 (46 000); and fVII-GlaEGF$_{NC}$, 13 950 (17 000).

Amidolytic Activity Measurements. The amidolytic activity of fVIIa (200 nM final concentration) was measured at room temperature in microtiter plates (Nunc). fVIIa was incubated in 50 mM HEPES (pH 7.4) containing 1.0 mM Ca^{2+}, 100 mM NaCl, 0.01% Tween 80, and various concentrations of GuHCl (Pierce) for 18−24 h before the amidolytic activity was measured by adding the chromogenic substrate S-2288 (Chromogenix). The initial rate of S-2288 cleavage was determined as ΔA_{405nm} per minute. A sample without fVIIa was used as the blank. In the temperature experiments, 0.4 mM S-2288 was added to 300 nM fVIIa which had been preincubated for 15 min at various (5−60 °C) fixed temperatures and the amidolytic activity of the reaction mixture was measured at the incubation temperature.

Intrinsic Fluorescence Measurements. Fluorescence measurements were performed using a Perkin-Elmer luminescence spectrometer (model LS 50 B). fVIIa and variants at a final concentration of 1 μM were incubated for 18−24 h in 0.1 M Tris-HCl (pH 7.5) containing various concentrations of GuHCl. Samples were excited at 295 nm to selectively monitor environmental changes around Trp residues. Fluorescence emission spectra were recorded between 310 and 450 nm using excitation and emission slits of 5 and 10 nm, respectively. To selectively excite the dansyl group in DEGR-fVIIa, an excitation wavelength of 340 nm and excitation and emission slits of 10 nm were used and the emission spectra were recorded between 400 and 650 nm.

Acrylamide Quenching of Fluorescence. Samples containing 1 μM protein were incubated for 18−24 h with three different concentrations of GuHCl (0, 1.0, and 5.0 M) buffered with 0.1 M Tris-HCl (pH 7.5). The fluorescence of the protein was quenched by the progressive addition of small aliquots of an 8 M acrylamide stock solution to a maximal concentration of 0.38 M. The Trp residues were excited at 295 nm, and quenching of the fluorescence was measured at the emission maximum. Identical results were obtained using the area under the emission peak. After corrections for dilution of samples, the quenching data were fitted to the modified form of the Stern−Volmer relationship (*18*):

$$F_0/F = (1 + K_{SV}[Q]) \exp(V[Q])$$

where F_0 and F are the fluorescence intensities in the absence and presence of the quencher, respectively, [Q] is the concentration of the quencher, K_{SV} is the dynamic quenching constant, and V is the static quenching constant.

Quasi-Elastic Light Scattering Measurements. Measurements of the translational diffusion coefficient of fVIIa were performed on a BI-2030AT 72 Channel Autocorrelator (Brookhaven Instrument Co., Holtsville, NY) operated in conjunction with a BI-200SM light scattering goniometer/photo counting detector and a Spectra Physics 127 He−Ne laser (60 mW, equipped with a vertical polarization rotator). Scattered light was collected at $\theta = 90°$. The scattering cuvette containing the sample was immersed in a refractive index matching medium. The temperature was controlled to an accuracy of ±0.1 °C. All buffers were filtered through a 0.22 μm Millipore filter. Buffer conditions were 100 mM NaCl and 20 mM HEPES (pH 7.4) with 5 mM $CaCl_2$. The z-averaged translational diffusion coefficient, D, was obtained from the intensity-normalized photo count autocorrelation function (*19*, *20*). The diffusion coefficient was determined from the slope of the reciprocal decay time Γ versus $\sin^2(\Theta_S/2)$,

$$\Gamma = K^2 D$$

where K is the scattering vector defined by

$$K = 4\pi n \sin(\Theta_S/2)/\lambda$$

The size distribution of fVIIa was analyzed using BI-MSDILT software, which was based on the exponential sampling technique and provided by Brookhaven Instrument Co. Decay times were calculated from the second-order cumulative expansion method (*21*). The accuracy of the polarized light scattering apparatus was checked using 0.1 μm and 0.6 μm Latex standards. Agreement was in both cases better that 2% for the hydrodynamic diameter.

Circular Dichroism Measurements. CD spectra were recorded on a CD6 spectrodichrograph (Jobin Yvon Instruments SA, Longjumeau, France) employing constant N_2 flushing. The instrument was calibrated using 10-camphorsulfonic acid (*22*). All experiments were performed in 20 mM HEPES (pH 7.5) and 150 mM NaCl. Thermal perturbation of the secondary structure of fVIIa and variants was measured by monitoring at 210 nm as a function of temperature. The protein concentration was 0.8−1.5 mg/mL. The sample was placed in a cuvette with a 1 mm path length, and the temperature of the chamber was raised from 25 to 70 °C using a heating rate of 1 °C/min using a thermoelectric cuvette holder. Thermal scans were performed using the same cell and cuvette holder by raising the temperature in 5 °C increments to 70 °C. The protein solution was allowed to equilibrate for 20 min at each temperature before the CD spectrum was recorded. Each spectrum was the result of three scans obtained by collecting data at 0.5 nm intervals with an integration time of 2 s. The spectra recorded at different GuHCl concentrations were obtained using a 0.01 cm cuvette as described (*23*). After baseline subtraction, a small degree of numerical (20−30% Savitsky−Golay) smoothing was applied. The observed ΔA values were converted to molar ϵ values on the basis of the molar concentration of the particular protein.

Differential Scanning Calorimetry Measurements. Calorimetric experiments were performed in the MC-2 differential scanning calorimeter from Microcal (Amherst, MA). The protein concentration ranged from 0.8 to 1.5 mg/mL. Samples were degassed for 5−10 min before being loaded into the calorimetric cell. The cell was pressurized with nitrogen to about 2.5 atm to prevent bubbling upon heating and loss of solvent by evaporation. All heating scans (15−110 °C) were recorded at the rate of 1 °C/min. Before each scan, the sample was equilibrated in the calorimetric cell for about 15 min at 15 °C. After the first scan, the sample was cooled and re-scanned to check the reversibility of the unfolding process. The melting curves were corrected for an instrument baseline obtained by heating a buffer sample. Melting temperatures (T_m), calorimetric enthalpies (ΔH_{cal}), and van't Hoff enthalpies (ΔH_{vH}) were calculated using the software MicroCal Origin version 2.9 (MicroCal Software, Inc.).

RESULTS

Factor VIIa Structure. The three-dimensional fVIIa structure is shown in Figure 1. It is based on the structure of fVIIa in complex with TF (*6*) and does not necessarily reflect the free fVIIa structure in solution. The overall structure is composed of four separate domains: the Gla domain, the first and second EGF-like domains, and the SP domain. fVIIa coordinates nine calcium ions: seven in the Gla domain coordinated by Gla residues, one in the first EGF-like domain, and one in the SP domain. The two fragments of fVIIa used in this study, des(1−44)-fVIIa which is composed of the two EGF-like and the SP domains and fVII-GlaEGF$_{NC}$ which is composed of the Gla domain and the two EGF-like domains, have been well characterized and are known to bind TF in a specific, Ca^{2+}-dependent manner (*7*, *16*).

GuHCl Stability Measurements on fVIIa and Variants. fVIIa contains eight Trp residues (*24*). Seven are located in the SP domain (Trp-166, Trp-187, Trp-201, Trp-284, Trp-356, Trp-364, and Trp-386), while one (Trp-41) is located at the interface between the Gla domain and the first EGF-like domain, in the hydrophobic stack (Figure 1). Hence, in des(1−44)-fVIIa, Trp-41 is deleted, leaving Trp residues only in the protease domain, and Trp-41 is the only tryptophan present in fVII-GlaEGF$_{NC}$. Discrete structural changes in the vicinity of the Trp residues in fVIIa can be measured by intrinsic Trp fluorescence using a selective excitation wavelength of 295 nm. The emission maximum of the indole rings is known to reflect the polarity of the local environment such that buried Trp residues in a nonpolar environment display a maximum at shorter wavelengths than exposed Trp residues. This relationship between the hydrophobicity of the environment and the emission maximum is utilized to monitor the denaturation process of fVIIa. Further, the use of fVIIa fragments allows the characterization of specific structural changes in the Gla and SP domains.

FIGURE 1: Ribbon diagram of fVIIa. It is color-coded as follows: des(1−44)-fVIIa, yellow and red; fVII-GlaEGF$_{NC}$, green and yellow; and fVIIa, green, yellow, and red. The location of the tryptophan residues is shown by white side chains, and the coordinated Ca^{2+} ions are shown by magenta balls. The picture was generated by ray-tracing using Quanta (Molecular Simulations, Inc., San Diego, CA), and the structure of fVIIa is taken from the complex with TF (*6*).

The emission maximum of fVIIa as a function of the GuHCl concentration is shown in Figure 2. The protein unfolds in two well-separated transitions when Ca^{2+} ions are present. The first transition occurs at about 0.3 M GuHCl and the second at 3 M GuHCl. The amidolytic activity vanishes in the first unfolding transition (data not shown),

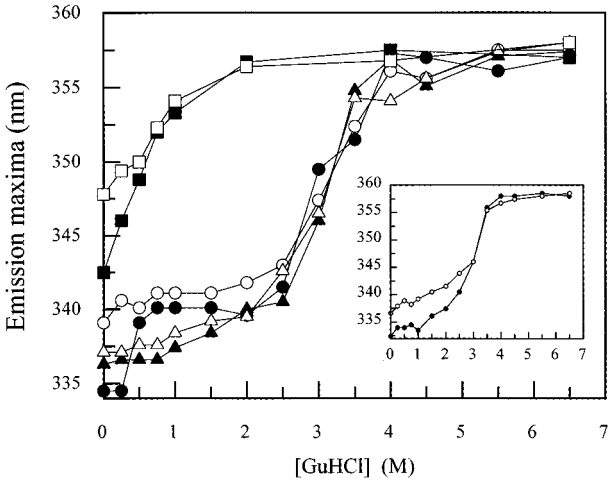

FIGURE 2: GuHCl-induced denaturation of fVIIa and variants monitored by intrinsic fluorescence. The emission maximum of fVIIa (●), des(1−44)-fVIIa (▲), and fVII-GlaEGF$_{NC}$ (■) as a function of the GuHCl concentration is shown (excitation at 295 nm). The protein concentration was 1 μM in 0.1 M Tris-HCl (pH 7.5), and the proteins were incubated with GuHCl for 24 h at room temperature. The inset shows the results for FFR-fVIIa. Filled symbols represent experiments performed in the presence of 5 mM Ca^{2+} and open symbols those without Ca^{2+}.

Table 1: Fluorescence Emission Wavelength Maxima and Intensity Changes for fVIIa and Variants at Different GuHCl Concentrations

variant		0 M GuHCl	1 M GuHCl	5 M GuHCl
fVIIa	Ca^{2+}	335 ± 2[a]	340 ± 1 (+24%)[b]	356 ± 2 (−1%)
	EDTA	338 ± 1 (+45%)	340 ± 1 (+38%)	354 ± 2 (+7%)
des(1−44)-fVIIa	Ca^{2+}	336 ± 1	337 ± 2 (−5%)	355 ± 2 (−7%)
	EDTA	336 ± 2 (+1%)	338 ± 3 (0%)	356 ± 1 (−4%)
fVIIa-GlaEGF$_{NC}$	Ca^{2+}	344 ± 3	353 ± 1 (+6%)	356 ± 1 (+41%)
	EDTA	348 ± 1 (+10%)	353 ± 1 (+7%)	356 ± 1 (+62%)
FFR-fVIIa	Ca^{2+}	333 ± 1	334 ± 1 (+17%)	356 ± 1 (−13%)
	EDTA	335 ± 1 (+45%)	337 ± 1 (+38%)	354 ± 2 (+3%)

[a] The wavelength maxima in nanometers are mean values with standard mean deviations and are based on triplicate experiments. [b] The numbers in parentheses indicate the relative increase or decrease in intensity of the emission peak compared to that of the native variant in the presence of Ca^{2+}.

indicating that structural changes in or around the active site take place during this event. In the absence of Ca^{2+}, the first transition disappears while the second transition remains. This indicates that Ca^{2+} binds to fVIIa and stabilizes a structure responsible for the first unfolding transition measured using fluorescence. The tryptophan emission spectrum in the absence of GuHCl is substantially quenched (reduced by 31%) and blue-shifted by 3 nm when Ca^{2+} is coordinated to fVIIa (Table 1). This massive reduction in fluorescence by Ca^{2+} is not observed at 1.0 M GuHCl, indicating that the region responsible for the Ca^{2+}-induced quenching in the native state of fVIIa is distorted and perhaps unable to bind Ca^{2+} at this moderate concentration of GuHCl.

To investigate the unfolding process in greater detail, truncated variants of fVIIa lacking individual domains were used. In des(1−44)-fVIIa, the Gla domain and part of the hydrophobic stack, including Trp-41, are removed. Consequently, this variant contains the seven Trp residues in the SP domain, and they are treated as a homogeneous population when monitoring structural changes in the SP domain. Only one unfolding transition is found for des(1−44)-fVIIa, coinciding with the second transition of full-length fVIIa (Figure 2), suggesting that this transition corresponds to the global unfolding of the SP domain in fVIIa. The amidolytic activity of des(1−44)-fVIIa disappears at the same GuHCl concentration as that of fVIIa, although no transition could be detected by a fluorescence change. The increase in fluorescence emission and accompanying red shift observed with fVIIa when going from 0 to 1.0 M GuHCl in the presence of Ca^{2+} are absent in des(1−44)-fVIIa. This indicates that the Ca^{2+}-dependent structure responsible for the quenching of Trp-41 fluorescence is disrupted in the first unfolding transition. Moreover, Ca^{2+} does not affect the fluorescence emission spectrum of des(1−44)-fVIIa at any GuHCl concentration (Table 1). The calcium binding site(s) influencing the intensity of the fluorescence emission spectrum of fVIIa is therefore likely to be located near Trp-41, presumably among the multiple Ca^{2+} binding sites in the Gla domain or the single Ca^{2+} site in the first EGF-like domain (*16*).

To confirm this conclusion, the stability of fVII-GlaEGF$_{NC}$ was studied. This fragment is composed of the Gla domain and the two EGF-like domains with a single Trp residue in position 41. Only one transition was detected, corresponding to the first unfolding transition detected for fVIIa (Figure 2). This unambiguously shows that the first transition in fVIIa represents the unfolding of the Gla domain and that the second transition reflects the unfolding of the SP domain. No evidence for an unfolding of the EGF-like domains was obtained. In addition, the Ca^{2+}-induced fluorescence quenching detected for fVIIa under native conditions is also found for fVII-GlaEGF$_{NC}$ (Figure 2 and Table 1), although to a lower extent, indicating that quenching is a consequence of Ca^{2+} binding either to the Gla domain or to the first EGF-like domain close to Trp-41. As for fVIIa, the emission spectrum of fVII-GlaEGF$_{NC}$ is blue-shifted 4 nm upon Ca^{2+} binding. This shows that Ca^{2+} binding moves Trp-41 into a more hydrophobic environment. This supports the idea that Ca^{2+} stabilizes the region around Trp-41 in the fVIIa structure responsible for the first GuHCl-induced unfolding transition of fVIIa. For fVIIa and the two variants, the emission maximum at high GuHCl concentrations is at 355−357 nm (Figure 2), indicating that the tryptophan residues are solvent-exposed under strongly denaturing conditions.

fVIIa can be inactivated by incorporation of peptide chloromethyl ketones in the active site. These inhibitors are known to induce subtle structural changes in the SP domain and to increase the affinity for TF (*14*, *25*). Irreversible serine protease inhibitors have also been shown in some cases to have a stabilizing effect (*26*). The inset in Figure 2 shows the results of stability measurements with inactivated fVIIa in the presence and absence of Ca^{2+}. Notably, in the presence of Ca^{2+}, the first transition is shifted to a higher GuHCl concentration compared to that for fVIIa and starts about 1 M GuHCl, while the second unfolding transition is unaffected. In the absence of Ca^{2+}, the transition profile for FFR-fVIIa is very similar to that of des(1−44)-fVIIa.

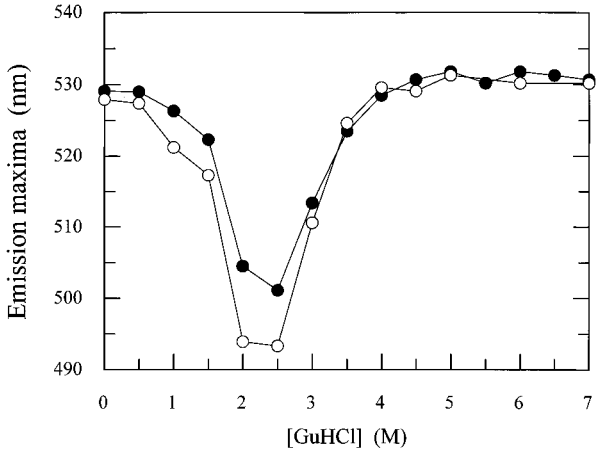

FIGURE 3: GuHCl-induced denaturation of DEGR-fVIIa monitored by dansyl fluorescence. The emission maximum as a function of the GuHCl concentration is shown (excitation at 340 nm). The protein concentration was 1 μM in 0.1 M Tris-HCl (pH 7.5), and the protein was incubated with GuHCl for 24 h at room temperature. Filled symbols represent results obtained with 5 mM Ca^{2+} and open symbols those without Ca^{2+}.

These data suggest that the active-site inhibitor is stabilizing the structure whose unfolding affects Trp-41 in the region between the Gla domain and the first EGF-like domain.

To specifically detect changes in the vicinity of the active site, the fluorescence emission maximum as a function of GuHCl concentration was measured for DEGR-fVIIa (Figure 3). DEGR-fVIIa harbors a dansyl group close to the active center that can be excited at 340 nm, and the resulting emission spectrum reflects the hydrophobicity of the environment of the dansyl group. In the native state, the dansyl group seems to be in a solvent-exposed environment on the basis of the red-shifted emission spectrum. Around 1 M GuHCl, a large blue shift takes place, indicating that the dansyl group becomes buried in a more hydrophobic environment. This transition corresponds to the small transition seen for FFR-fVIIa around 1 M GuHCl (inset of Figure 2). Hence, both inhibitors seem to stabilize the first unfolding transition detected for fVIIa. A second transition (a large red shift) is detected at about 3 M GuHCl (Figure 3), coinciding with the global unfolding of the SP domain (Figure 2). The emission maximum value at high GuHCl concentrations is similar to that of the native state, showing that the dansyl group becomes solvent-exposed to the same extent as it does in the native state. It is also important to note that Ca^{2+} has a very small influence on both transitions (Figure 3), i.e., on the active-site structure in the native and intermediate states.

CD Measurements of fVIIa and Variants at Various GuHCl Concentrations. Far-UV CD spectra were recorded to distinguish between a local rearrangement in the vicinity of Trp-41 and a more global unfolding of the surrounding structure detected during the first GuHCl-induced transition (Figure 2). Figure 4 shows the far-UV spectra of fVIIa, des-(1−44)-fVIIa, and fVII-GlaEGF$_{NC}$ at 0, 1.5, and 5 M GuHCl, respectively. A detectable change in the spectrum of fVIIa is seen at 1.5 M GuHCl compared to the spectrum of the native protein. At 5 M GuHCl, the spectrum is typical for an unordered structure. In des(1−44)-fVIIa, there is only a small difference between the native spectrum and the spectrum obtained at 1.5 M GuHCl, indicating that only

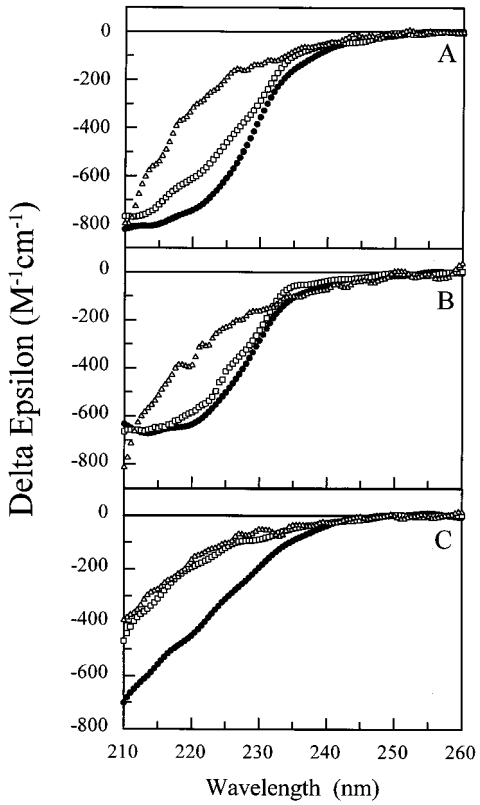

FIGURE 4: Far-UV CD spectra of fVIIa and variants at different GuHCl concentrations. Measurements were carried out with fVIIa (A), des(1−44)-fVIIa (B), and fVII-GlaEGF$_{NC}$ (C) after incubation for 24 h at room temperature in the presence of 0 (●), 1.5 (□), and 5 M (△) GuHCl. The protein concentration was between 0.4 and 1.2 mg/mL in buffer containing 5 mM $CaCl_2$.

minor structural changes take place. On the other hand, a large change in the CD spectrum is noted for fVII-GlaEGF$_{NC}$, suggesting an unfolded Gla domain structure at 1.5 M GuHCl. Notably, the effect induced by 1.5 M GuHCl is very similar to that observed when Ca^{2+} is removed from these protein variants (*23*). This supports the conclusion that the global unfolding of the Gla domain takes place in the first GuHCl-induced transition, while the SP domain remains in a globular state with native secondary structure but lacks enzymatic activity. The SP domain is subsequently unfolded between 1.5 and 5 M GuHCl.

Quenching of Intrinsic Fluorescence by Acrylamide. Quenching of Trp fluorescence at 0, 1, and 5 M GuHCl by the addition of acrylamide was measured to investigate the degree of solvent exposure of the Trp residues in the native, intermediate, and unfolded state of the protein, respectively. Stern−Volmer plots of the results are shown in Figure 5. A larger slope in the Stern−Volmer plot reflects an increased average Trp exposure to the solvent. Overall, a gradual increase in acrylamide quenching is seen for the fVIIa variants when the GuHCl concentration is increased, especially from 1 to 5 M. Ca^{2+} binding to fVIIa has only a minor effect on the ability of acrylamide to quench exposed Trp residues. Trp-41 in fVII-GlaEGF$_{NC}$ seems to be relatively more exposed at 1 M GuHCl compared to other Trp residues in fVIIa both in the presence and in the absence of Ca^{2+}. The inhibitor in FFR-fVIIa seems to reduce the exposure of Trp residues in fVIIa independent of Ca^{2+}.

Thermal Denaturation of fVIIa and Variants Measured by CD. To investigate thermally induced effects on the various

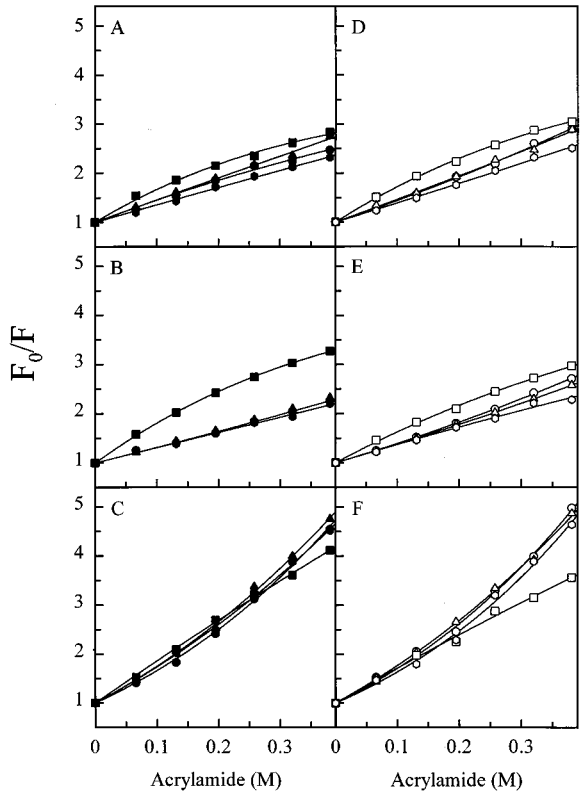

FIGURE 5: Stern−Volmer plots of the acrylamide quenching of the intrinsic fluorescence of fVIIa and variants. fVIIa (●), des(1−44)-fVIIa (▲), fVII-GlaEGF$_{NC}$ (■), and FFR-fVIIa (⬢) were incubated with 0 (A and D), 1 (B and E), and 5 M (C and F) GuHCl. The filled symbols in panels A−C represent results obtained in the presence of 5 mM Ca^{2+} and the open symbols in panels D−F those without Ca^{2+}. F_0, the fluorescence intensity in the absence of acrylamide, is arbitrarily set to 1, and F is the intensity in the presence of acrylamide.

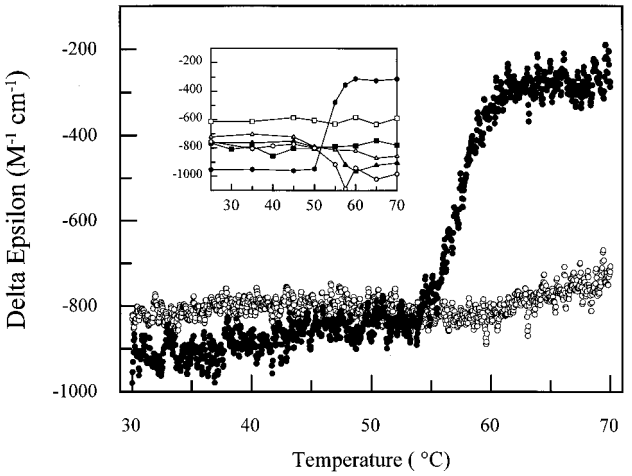

FIGURE 6: Thermal denaturation of fVIIa and variants monitored by far-UV CD. The ellipticity at 210 nm as a function of temperature is shown for fVIIa (●). The inset shows the results for des(1−44)-fVIIa (▲), fVII-GlaEGF$_{NC}$ (■), and FFR-fVIIa (⬢). Filled symbols show the results obtained with Ca^{2+}-loaded proteins (5 mM) and open symbols those obtained with the apo forms. The protein concentration was between 0.8 and 1.5 mg/mL.

domains in fVIIa, secondary structural changes were studied by measuring CD at 210 nm where the spectrum of fVIIa has its minimum (*23*). Figure 6 shows the thermostability of fVIIa in the presence and the absence of Ca^{2+}. Results identical to those monitored at 210 nm were obtained when the CD spectrum between 205 and 260 nm was recorded at various fixed temperatures (data not shown). In the presence of Ca^{2+}, one transition is found with a midpoint temperature (T_m) of 58 °C, indicating that secondary structural changes occur at that temperature. On the other hand, no transition was detected in the absence of Ca^{2+}. The thermal stability of the two fragments of fVIIa was also measured (inset of Figure 6). For fVII-GlaEGF$_{NC}$, no transition was found between 25 and 70 °C either in the presence or in the absence of Ca^{2+} ions. The negative ϵ value at 210 nm for fVII-GlaEGF$_{NC}$ is larger in the presence of Ca^{2+} than in its absence, suggesting that calcium stabilizes a more ordered structure of this fragment, in agreement with earlier measurements (*23*). No unfolding transition was detected for des-(1−44)-fVIIa (inset of Figure 6) even though this fVIIa fragment only lacks the 44 N-terminal amino acids. Taken together, the presence of both the SP domain and the Gla domain is a prerequisite for the detection of a cooperative unfolding transition between 55 and 60 °C in the presence of Ca^{2+}.

FFR-fVIIa has an unfolding transition similar to that of fVIIa in the presence of Ca^{2+}, but with a slightly lower T_m value (inset Figure 6). This indicates that the inhibitor destabilizes the secondary structure of fVIIa. This is an unexpected result considering the fact that chloromethyl ketone inhibitors are generally known to have a stabilizing effect on serine proteases (*26*). As with fVIIa, no unfolding transition was detected with FFR-fVIIa when Ca^{2+} ions were removed.

Thermal Denaturation of fVIIa and Variants Measured by DSC. In the presence of Ca^{2+}, fVIIa exhibited a heat absorption peak in the temperature range where we observed an ϵ change in the CD measurements (Figure 7A). Under the conditions used, the unfolding transition was irreversible since the peak could not be reproduced when the protein was heated a second time (data not shown). The T_m value and calorimetric enthalpy of the transition were 58.1 °C and 166 kcal/mol, respectively (Table 2). The enthalpy value obtained for fVIIa is similar to that of protein C and factor IX (*11*, *12*). When Ca^{2+} was removed from fVIIa, the enthalpy value was reduced by half and the T_m value decreased by 2.7 °C. This was also seen for protein C and factor IX, and the calorimetric enthalpy value obtained in the absence of Ca^{2+} is close to those reported for other serine proteases (*26*). This suggests that Ca^{2+} coordination induces a more compact fVIIa structure, primarily in the Gla domain, and this is responsible for the Ca^{2+}-induced calorimetric enthalpy change of fVIIa. This interpretation was confirmed with des(1−44)-fVIIa. Compared to fVIIa, this derivative was shown to unfold at a similar T_m value but with a reduced calorimetric enthalpy value equivalent to that obtained for fVIIa in the absence of Ca^{2+} (Table 2). In addition, the enthalpy value of des(1−44)-fVIIa was not affected by Ca^{2+}. The T_m values for fVIIa and des(1−44)-fVIIa in the absence of Ca^{2+} are lower than those in its presence, indicating that Ca^{2+} binding to the SP domain increases its stability slightly. With the fVII-GlaEGF$_{NC}$ fragment (lacking the SP domain), no melting transition was found when it was heated to 110 °C even in the presence of Ca^{2+} (data not shown). This implies that the enthalpy contribution from the Ca^{2+}-saturated Gla domain in fVIIa is somehow dependent on the presence of the SP domain. The calorimetric to van't Hoff enthalpy

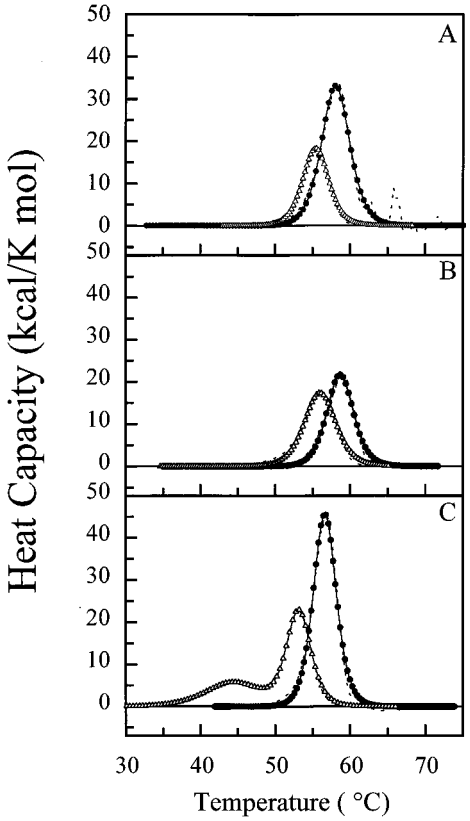

FIGURE 7: DSC curves of fVIIa and variants. Panels A−C show the thermograms of fVIIa, des(1−44)-fVIIa, and FFR-fVIIa, respectively. Filled symbols represent experiments performed in the presence of 5 mM Ca^{2+} and open symbols those without Ca^{2+}. All experiments were performed in 20 mM HEPES (pH 7.5) and 150 mM NaCl. Dashed lines represent experimental data, and solid lines represent the best fit to a non-two-state transition.

Table 2: Thermodynamic Parameters of the Melting Process of fVIIa and Variants[a]

	Ca^{2+}			EDTA		
	T_m	ΔH_{cal}	$\Delta H_{cal}/\Delta H_{vH}$	T_m	ΔH_{cal}	$\Delta H_{cal}/\Delta H_{vH}$
fVIIa	58.1	166	0.95	55.4	84	0.45
des(1−44)-fVIIa	58.7	102	0.55	56.0	97	0.63
FFR-fVIIa	56.6	186	0.88	53.2	96	0.52
				44.5	59	0.65

[a] T_m is given in degrees Celsius, and ΔH is given in kilocalories per mole.

ratios are substantially less than unity in the absence of Ca^{2+} (Table 2), indicating that aggregation or some other process influences the shape of the heat absorption peak.

The thermograms of FFR-fVIIa displayed a single transition in the presence of Ca^{2+} (Figure 7C). The heat enthalpy for FFR-fVIIa is somewhat larger than that for fVIIa, and the thermal transition becomes more narrow. This was also found for a chloromethyl ketone-inhibited form of protein C (*11*). In agreement with the CD measurements, the T_m value decreased by 1.5 °C compared to that of fVIIa (Table 2). The thermogram differed markedly when FFR-fVIIa was heated in the absence of Ca^{2+}. Apart from the main peak at 53.2 °C, an additional melting peak was detected with a T_m value of 44.5 °C, and this transition was apparently less cooperative compared to the main peak. The sum of the heat enthalpies of these two peaks (155 kcal/mol) is less than the single transition found in the presence of Ca^{2+} (Table 2). This shows that Ca^{2+} also increases the heat enthalpy for FFR-fVIIa, but the Ca^{2+} effect on the calorimetric enthalpy is smaller for FFR-fVIIa than for fVIIa (31 compared to 82 kcal/mol).

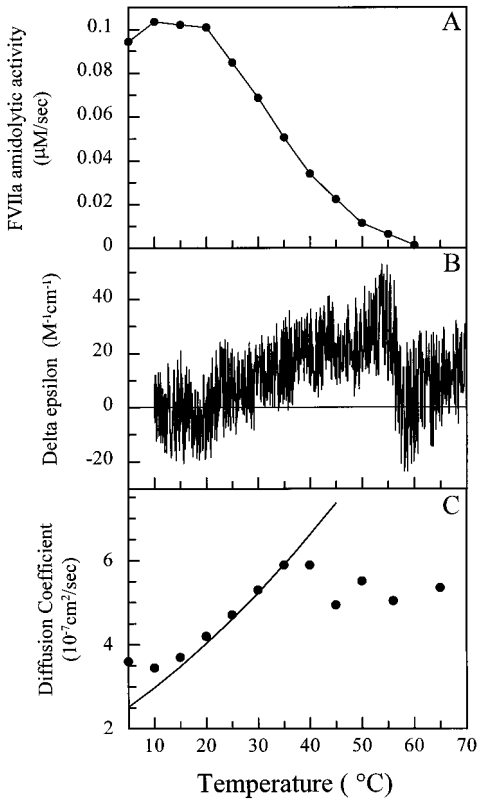

FIGURE 8: Amidolytic activity, near-UV CD, and diffusion coefficient of Ca^{2+}-loaded fVIIa as a function of temperature. (A) The amidolytic activity of fVIIa, measured as the release of *p*-nitroaniline from the substrate S-2288, as a function of temperature. (B) Changes in the near-UV CD spectrum of fVIIa at 293 nm as a function of temperature. (C) Changes in the diffusion coefficient of fVIIa as a function of temperature. The solid line represents changes in the molecular shape modeled by a prolate ellipsoid with an axial ratio of 2.3.

Subtle Structural Changes in fVIIa. Even though the major structural changes in fVIIa occur at a relatively high temperature (Figures 6 and 7), the activity (not shown) and fluorescence data in GuHCl (Figures 2 and 3) indicate that the active site is disrupted before the global unfolding of the SP domain occurs. We therefore decided to look for minor structural changes in fVIIa of possible physiological relevance. The thermal effect on the amidolytic activity of fVIIa is shown in Figure 8A. The amidolytic activity decreased almost linearly with increasing temperature with a half-maximum at about 30 °C. Hence, fVIIa has a low amidolytic activity at physiological temperature. Interestingly, the shape of the curve changed when the measurement was performed in the presence of soluble TF, being a bell-shaped curve with maximal activity at 30 °C (data not shown). Also worth mentioning is the fact that the loss of activity is completely reversible up to about 55 °C; i.e., fVIIa regains its amidolytic activity when cooled unless the temperature has exceeded 55 °C.

Near-UV CD is a powerful technique that can be used for probing small structural changes. The near-UV region reflects the tertiary structure and is therefore a fingerprint of the native state of a protein (*27*). The spectrum mainly

reflects the asymmetric environment of the aromatic residues, and recent studies have shown that Trp residues display strong CD bands in this region (*28*, *29*). Figure 8B shows the thermal effect on fVIIa measured by the change in $\Delta\epsilon$ at 293 nm, which represents one of the two predominant vibrational bands in the near-UV CD spectrum (*23*). The signal-to-noise ratio is relatively low because of the low amplitude of this CD band. The $\Delta\epsilon$ value increases gradually up to about 55 °C, and then there is a rapid decrease. This decrease probably reflects the unfolding event also detected in the far-UV CD and DSC measurements (Figures 6 and 7). The slow increase in $\Delta\epsilon$ follows the same pattern as the loss of amidolytic activity (Figure 8A).

To monitor the global shape of fVIIa in solution, we also measured the diffusion coefficient as a function of temperature. It can be seen in Figure 8C that fVIIa initially becomes apparently smaller in size when the temperature is increased, but above 50 °C, fVIIa becomes apparently larger, i.e., more extended. This is in agreement with the major unfolding transition seen in CD and DSC measurements. In the temperature interval of 20−40 °C, the molecular shape can be modeled by a prolate ellipsoid with an axial ratio of 2.3.

DISCUSSION

This report presents the characterization of the stability of fVIIa and two derivatives of fVIIa, each lacking one domain. Using GuHCl-induced and thermal unfolding experiments, we studied unfolding of separate domains and also address the issue of domain−domain interactions. In addition, the effect of Ca^{2+} and an active-site inhibitor on the stability was analyzed. We know from biochemical studies (reviewed in ref *5*) and from the X-ray structure determination of the fVIIa−soluble TF complex (*6*) that the complex formation is a multidomain binding event. From a study of the interaction between soluble TF and fVIIa (*23*), we also know that binding to TF induces structural changes in the SP domain of fVIIa. This enhances the catalytic efficiency of fVIIa and thereby initiates the coagulation cascade. A complete understanding of the molecular mechanism of fVIIa activation by binding to TF has however been precluded by the lack of structural information about the free form of fVIIa. A better understanding of interdomain interactions and intrinsic domain stability within fVIIa may illuminate the mode of function of fVIIa and the mechanism of fVIIa−TF complex formation.

We have shown that fVIIa unfolds in two well-separated transitions as monitored by intrinsic fluorescence when using GuHCl as the denaturant. The fluorescence changes reflect an altered environment in the vicinity of Trp residues. With carbonic anhydrase (*30*), it has been possible to assign specific fluorescence properties to individual Trp residues in the protein. Hydrophobicity and quenching capability are two properties of the Trp environment that affect the wavelength maximum and intensity of the emission spectrum. Quenching and a small blue shift of the emission spectrum are seen when fVIIa binds Ca^{2+} (Figure 2 and Table 1). No quenching was detected with des(1−44)-fVIIa, indicating that Trp-41 is affected by binding of Ca^{2+}, and this was corroborated by the Ca^{2+} effect on Trp-41 in the fVII-$GlaEGF_{NC}$ fragment in this work and a previous study (*16*). On the basis of results with factor X (*31*), the underlying conformational change most likely results from Ca^{2+} binding to the Gla domain. In the X-ray structure of fVIIa in complex with soluble TF, the distance from Trp-41 to one obvious quenching candidate, Lys-38, is 9 Å, and it has been shown that charged residues are efficient quenchers. Another possible quenching event that has been proposed is the interaction between Trp-41 and the nearby Cys-17−Cys-22 disulfide bond (*32*). Calhoun et al. (*33*) found that the fluorescence from solvent-exposed Trp residues is more effectively quenched by acrylamide than that from buried Trp residues; i.e., acrylamide does not readily penetrate native protein structures. We used this approach to monitor the exposure of Trp residues in fVIIa under different conditions (Figure 5) and were unable to detect a significant Ca^{2+} effect on the native state of fVIIa in this respect. The Ca^{2+} effect on the intrinsic fluorescence of fVIIa disappears after the first unfolding transition around 0.3 M GuHCl. This strongly supports the interpretation that the Ca^{2+} binding site responsible for the quenching of Trp-41 is disrupted in the intermediate state of fVIIa between 0.5 and 2.5 M GuHCl. The far-UV CD data (Figure 4) are in agreement with this conclusion and suggest that the Gla domain (fVII-$GlaEGF_{NC}$) is highly unordered at the intermediate GuHCl concentration while the SP domain [des(1−44)-fVIIa] is native-like. Interestingly, the Gla domain in fVIIa unfolds at the GuHCl concentration required to abolish the amidolytic activity. This raises the possibility of an interplay between the Gla and SP domains. However, the unfolding of the Gla domain in fVII-$GlaEGF_{NC}$ and the loss of the amidolytic activity of des(1−44)-fVIIa occur at the same GuHCl concentration, indicating that this could be a coincidence. The Ca^{2+} dependence of the fVIIa amidolytic activity indicates that a Ca^{2+}-loaded and structurally ordered Gla domain is required for full activity (*16*), suggesting not only an interaction between the Gla and SP domains but also an influence of the Gla domain on the activity of fVIIa. This point is strengthened by the stability data on FFR-fVIIa which show that the first GuHCl-induced transition, corresponding to the unfolding of the Gla domain, is stabilized by incorporation of the inhibitor into the SP domain. The SP domain is composed of two subunits that divide the domain into two lobes. The incorporated inhibitor is covalently attached to two active-site residues (His-193 and Ser-344), one in each subunit. This linkage conceivably stabilizes the interface between the subunits and makes the SP domain more resistant against GuHCl-induced denaturation. A disruption of the interface between the subunits in the SP domain of fVIIa splits the catalytic triad, resulting in the loss of amidolytic activity in the first GuHCl-induced transition. The results with DEGR-fVIIa, which has a fluorescent dansyl group attached close to the active site, show the same two transitions observed with FFR-fVIIa. Thus, both transitions affect the environment of the dansyl moiety. In the first transition, the dansyl group is transferred to a more hydrophobic environment (Figure 3). This might be accomplished by insertion of the hydrophobic dansyl group into the apolar environment between the subunits of the SP domain. In the second transition, the subunits in the SP domain unfold and the dansyl group becomes solvent-exposed to the same extent as it is in the native state. The proposed subunit separation in the first unfolding transition might also contribute to the

unfolding of the Gla domain by disrupting the Gla domain-interacting surface on the SP domain. This would explain the simultaneous loss of amidolytic activity and unfolding of the Gla domain.

To probe the thermal stability of individual domains in fVIIa, far-UV CD was measured as a function of temperature at a wavelength corresponding to the minimum in the fVIIa spectrum (*23*). Thermal unfolding of fVIIa occurs cooperatively in the presence of Ca^{2+} with a T_m of around 58 °C (Figure 6). No transition was detected in the absence of Ca^{2+}. Interestingly, no unfolding transition is detected when either the Gla or the SP domain is missing, even in the presence of Ca^{2+}. This raises the question of whether Ca^{2+} maintains fVIIa in a conformational state where the Gla domain associates with the SP domain. The Gla domain in fVIIa is composed of three small α-helices (*6*). The domain is more flexible in the absence of Ca^{2+}, resembling a molten globule structure (*34*), and Ca^{2+} binding to fVIIa predominantly orders the α-helical structures in the Gla domain (*23*). As mentioned above, the unfolding of this region in fVIIa could be detected by fluorescence changes of Trp-41 and by far-UV CD. However, no heat absorption could be detected for fVII-GlaEGF$_{NC}$ by calorimetry during thermal unfolding even in the presence of Ca^{2+}. It has been shown with factor IX that the EGF-like domains are extremely stable at neutral pH and their unfolding was only detected when lowering the pH to 3.5 (*12*). At this pH, no melting transitions were detected with fVIIa up to 110 °C (data not shown). A possible explanation for the results with fVII-GlaEGF$_{NC}$ is that the Gla domain is small and, in contrast to the characteristic feature of globular proteins with a tight packing of nonpolar side chains forming the inside of the protein, has a polar interior in the presence of Ca^{2+} with the apolar residues located on the surface (*34*, *35*). This is mainly due to the network of nine negatively charged Gla residues binding seven Ca^{2+} ions in the interior of the domain. The lower limit of the size of a cooperative domain has been estimated to be approximately 50 residues at physiological temperature (*36*). This is determined by the requirement that it should be stable with an organized structure. Exceptions, such as the well-defined NMR structure of a 35-residue subdomain from villin with a tightly packed hydrophobic core (*37*), have been described in the literature. The Gla domain including the hydrophobic stack (45 residues) presumably fulfils the size requirement, but its unusual structure explains the lack of heat absorption during denaturation. In contrast, in intact fVIIa, i.e., in the presence of the SP domain, the Gla domain contributes significantly to the calorimetric enthalpy. The enthalpy contribution from the Gla domain is also dependent on Ca^{2+} (Table 2), again showing the importance of Ca^{2+} binding to the Gla domain. The large enthalpy contribution from the Gla domain (64 kcal/mol) is probably due to the exposure of surfaces involved in an interaction between the Gla and SP domains rather than due to the unfolding of the Gla domain itself. The calorimetric results are in agreement with the GuHCl stability data presented above. Using calorimetry, it was recently suggested that the SP domain and the Gla domain in protein C interact (*11*). These data and ours suggest a high degree of flexibility within protein C and fVIIa and that the properties of individual domains can be strongly influenced by interactions with other parts of the protein. For small compact globular proteins, the effective van't Hoff enthalpy of denaturation is found to be in good agreement with the calorimetric enthalpy, such that denaturation can be regarded as a two-state transition (*38*). For fVIIa, there is a large discrepancy between the effective van't Hoff enthalpy and the actual calorimetric enthalpy of denaturation, especially in the absence of Ca^{2+} (Table 2). Denaturation of fVIIa and variants thereof appears not to represent a simple two-state transition. A $\Delta H_{cal}/\Delta H_{vH}$ ratio of less than unity reflects the influence of aggregation or some other process on the shape of the heat absorption peak.

There are three different Ca^{2+} binding regions in fVIIa: the Gla domain where seven Ca^{2+} ions coordinate, the first EGF-like domain where one Ca^{2+} binds, and one Ca^{2+} site in the SP domain (*6*). Ca^{2+} binding to the sites in the Gla and first EGF-like domains has been shown to be vital for the tight binding to TF (*7*, *9*, *39*, *40*), and the site in the SP domain is involved in fVIIa activity (*40*, *41*). This study shows that binding of Ca^{2+} to the SP domain increases the melting temperature by 2.7 °C and the calorimetric enthalpy by 5 kcal/mol (Table 2). It is unlikely that the slightly enhanced thermal stability afforded by Ca^{2+} plays an important physiological role for fVIIa. However, the removal of Ca^{2+} in vitro might cause a repulsive effect between the negatively charged carboxyl groups in the loop in the SP domain involved in Ca^{2+} binding, resulting in a destabilization of this domain and, in turn, the whole protein. Interestingly, chemical cross-linking has shown that, after complex formation between fVIIa and TF, Ca^{2+} binding to the SP domain or any other site in fVIIa is not essential for the amidolytic activity of fVIIa (*42*). This indicates that Ca^{2+} binding to the SP domain is not important for the catalytic activity of fVIIa when it is bound to TF. A Ca^{2+} binding site in a mesophilic xylanase was shown to be important for the protection of the enzyme against proteolytic attack but not to be involved in enzyme activity and stability (*43*).

Interestingly, subtle structural changes occur in fVIIa prior to the temperature-induced global unfolding detected using far-UV CD and DSC. Virtually no amidolytic activity of fVIIa remains at 50 °C, and concomitant structural changes were observed in the near-UV CD analysis (Figure 8). The loss of amidolytic activity is totally reversible in the temperature region below 55 °C, also indicating that small structural changes take place before the major unfolding transition occurs around 58 °C. The change in the near-UV CD signal at 293 nm is quite unexpected (Figure 8B). This signal reflects the degree of asymmetry sensed by the aromatic residues, especially Trp residues, and is directly related to the tightness and specificity of the tertiary packing. The increased CD signal seen with increasing temperatures indicates that the Trp residues become more fixed, suggesting a more ordered and rigid tertiary structure. At present, we believe that a tighter hydrophobic interaction between the two subunits in the SP domain is responsible for this effect. The simultaneous loss of amidolytic activity might also be explained by the lower flexibility in the active site between the two SP domain subunits. A temperature-induced conformational change in fVIIa is reflected in the rather striking change in the diffusion coefficient of fVIIa. Little change is observed below 20 °C. Above 20 °C, the diffusion coefficient increases up to approximately 40 °C, indicating a transformation into a more compact molecule. This

probably reflects a stronger interaction between the SP domain and the Gla domain due to increasing hydrophobic interactions at higher temperatures.

ACKNOWLEDGMENT

We thank Annette Danielsen, Elke Gottfriedsen, Jeanette Lundqvist, and Anette Østergaard for excellent technical assistance. We also thank Dr. Ole H. Olsen (Novo Nordisk) for the creation of Figure 1, Dr. Uno Carlsson (Linköping University) for making a spectrodichrograph available to us, and Dr. Litian Fu (California Institute of Technology) for excellent help with the calorimetric measurements.

REFERENCES

1. Davie, E. W., Fujikawa, K., and Kisiel, W. (1991) *Biochemistry 30*, 10363−10370.
2. Furie, B., and Furie, B. C. (1988) *Cell 53*, 505−518.
3. Østerud, B., and Rapaport, S. I. (1977) *Proc. Natl. Acad. Sci. U.S.A. 74*, 5260−5264.
4. Silverberg, S. A., Nemerson, Y., and Zur, M. (1977) *J. Biol. Chem. 252*, 8481−8488.
5. Martin, D. M. A., Boys, C. W. G., and Ruf, W. (1995) *FASEB J. 9*, 852−859.
6. Banner, D. W., D'Arcy, A., Chène, C., Winkler, F. K., Guha, A., Konigsberg, W. H., Nemerson, Y., and Kirchhofer, D. (1996) *Nature 380*, 41−46.
7. Persson, E. (1997) *FEBS Lett. 413*, 359−363.
8. Neuenschwander, P. F., and Morrissey, J. H. (1994) *J. Biol. Chem. 269*, 8007−8013.
9. Sabharwal, A. K., Birktoft, J. J., Gorka, J., Wildgoose, P., Petersen, L. C., and Bajaj, S. P. (1995) *J. Biol. Chem. 270*, 15523−15530.
10. Ashton, A. W., Kemball-Cook, G., Johnson, D. J. D., Martin, D. M. A., O'Brien, D. P., Tuddenham, E. G. D., and Perkins, S.J. (1995) *FEBS Lett. 374*, 141−146.
11. Medved, L. V., Orthner, C. L., Lubon, H., Lee, T. K., Drohan, W. N., and Ingham, K. C. (1995) *J. Biol. Chem. 270*, 13652−13659.
12. Vysotchin, A., Medved, L. V., and Ingham, K. C. (1993) *J. Biol. Chem. 268*, 8436−8446.
13. Thim, L., Bjoern, S., Christensen, M., Nicolaisen, E. M., Lund-Hansen, T., Pedersen, A., and Hedner, U. (1988) *Biochemistry 27*, 7785−7793.
14. Sørensen, B. B., Persson, E., Freskgård, P.-O., Kjalke, M., Ezban, M., Williams, T., and Rao, L. V. M. (1997) *J. Biol. Chem. 272*, 11863−11868.
15. Nicolaisen, E. M., Petersen, L. C., Thim, L., Jacobsen, J. K., Christensen, M., and Hedner, U. (1992) *FEBS Lett. 306*, 157−160.
16. Persson, E., and Petersen, L. C. (1995) *Eur. J. Biochem. 234*, 293−300.
17. Pace, C. N., Vajdos, F., Fee, L., Brimsley, G., and Gray, T. (1995) *Protein Sci. 4*, 2411−2423.
18. Eftink, M. R., and Ghiron C. A. (1976) *J. Phys. Chem. 80*, 486−493.
19. Johnson, C. S., Jr., and Gabriel, D. A. (1995) *Dynamic Light Scattering*, Dover Publications, Inc., New York.
20. Berne, B. J., and Pecora, R. (1976) *Dynamic Light Scattering with Applications to Chemistry, Biology, and Physics*, Wiley-Interscience, New York.
21. Chu, B. (1974) in *Laser Scattering*, pp 231−236, Academic Press, New York.
22. Hennessey, J. P., and Johnson, W. C. (1982) *Anal. Biochem. 125*, 177−188.
23. Freskgård, P.-O., Olsen, O. H., and Persson, E. (1996) *Protein Sci. 5*, 1531−1540.
24. Hagen, F. S., Gray, C. L., O'Hara, P., Grant, F. J., Saari, G. C., Woodbury, R. G., Hart, C. E., Insley, M., Kisiel, W., Kurachi, K., and Davie, E. W. (1986) *Proc. Natl. Acad. Sci. U.S.A. 83*, 2412−2416.
25. Dickinson, C. D., and Ruf, W. (1997) *J. Biol. Chem. 272*, 19875−19879.
26. Novokhatny, V., Medved, L., Mazar, A., and Ingham, K. (1993) *J. Biol. Chem. 268*, 17211−17218.
27. Woody, R. W., and Dunker, A. K. (1996) in *Circular Dichroism and the Conformational Analysis of Biomolecules* (Fasman, G. D., Ed.) pp 109−157, Plenum Press, New York.
28. Vuillemier, S., Sancho, J., Loewenthal, R., and Fersht, A. R. (1993) *Biochemistry 32*, 10303−10313.
29. Freskgård, P.-O., Carlsson, U., Mårtensson, L.-G., Jonasson, P., and Jonsson, B.-H. (1994) *Biochemistry 33*, 14281−14288.
30. Mårtensson, L.-G., Jonasson, P., Freskgård, P.-O., Svensson, M., Carlsson, U., and Jonsson, B.-H. (1995) *Biochemistry 34*, 1011−1021.
31. Persson, E., Björk, I., and Stenflo, J. (1991) *J. Biol. Chem. 266*, 2444−2452.
32. Soriano-Garcia, M., Padmanabhan, K., de Vos, A. M., and Tulinsky, A. (1992) *Biochemistry 31*, 2554−2566.
33. Calhoun, B. D., Vanderkooi, J. M., Holtom, G. R., and Englander, S. W. (1986) *Proteins: Struct., Funct., Genet. 1*, 109−115.
34. Sunnerhagen, M., Forsén, S., Hoffrén, A. M., Drakenberg, T., Teleman, O., and Stenflo, J. (1995) *Nat. Struct. Biol. 2*, 504−509.
35. Freedman, S. J., Furie, B. C., Furie, B., and Baleja, J. D. (1995) *Biochemistry 34*, 12126−12137.
36. Privalov, P. L. (1992) in *Protein Folding* (Creighton, T. T., Ed.) pp 83−126, Freeman, New York.
37. McKnight, C. J., Matsudaira, P. T., and Kim, P. S. (1997) *Nat. Struct. Biol. 4*, 180−184.
38. Privalov, P. L. (1979) *Adv. Protein Chem. 33*, 167−182.
39. Persson, E., Olsen, O. H., Østergaard, A., and Nielsen, L. S. (1997) *J. Biol. Chem. 272*, 19919−19924.
40. Kelly, C. R., Dickinson, C. D., and Ruf, W. (1997) *J. Biol. Chem. 272*, 17467−17472.
41. Wildgoose, P., Foster, D., Schiødt, J., Wiberg, F. C., Birktoft, J. J., and Petersen, L. C. (1993) *Biochemistry 32*, 114−119.
42. Miyata, T., Funatsu, A., and Kato, H. (1995) *J. Biochem. 117*, 836−844.
43. Spurway, T. D., Morland, C., Cooper, A., Sumner, I., Hazlewood, G. P., O'Donnell, A. G., Pickersgrill, R. W., and Gilbert, H. J. (1997) *J. Biol. Chem. 272*, 17523−17530.

BI972847M